Short Communication

A Flower-Shape NiO/Co₃O₄ Composite as Anode for Lithium Ion Battery Prepared by a Template-Free Hydrothermal Method

Qian Liu[1,2], Guoxu Zheng[2,1,*], Jinghua Yin[1], Mingxin Song[4], Yang Wang[3], Shiyi Tian[3], Fengquan Zhang[5]

[1] School of Materials Science and Engineering, Harbin University of Science and Technology, Harbin 150080, P. R. China
[2] School of Soft and Microelectronic, Harbin University of Science and Technology, Harbin 150080, PR China
[3] School of Science, Harbin University of Science and Technology, Harbin 150080, PR China
[4] College of Applied Science and Technology, Hainan University, Haikou 570228, PR China
[5] No. 13 Middle School of Harbin, Harbin 150000, PR China
[*]E-mail: shandian2008.ok@163.com

To improve the performance of lithium ion batteries and super capacitors, various metal organic frameworks (MOFs) and their derivations have been used as electrode materials because of their large surface area and excellent structural characteristics. Among MOFs derivations, transition metal oxides (TMOs) have attracted increasing attention due to their high theoretical capacitance and excellent chemical stability. Mixed TMOs, which contains multiple metal cations, can significantly enhance the storage capacity of lithium ion and improve the conductivity and electrochemical reactivity. In this study, a NiO/Co_3O_4 composite material was prepared using a template-free hydrothermal method for lithium ion battery. The material's phase structure and morphology were characterized using X-ray diffraction and scanning electron microscopy. The results revealed that the composite material had a special flower-like morphology and was composed purely of rhombus NiO and cubic Co_3O_4. The electrochemical performance of the NiO/Co_3O_4 composite material was tested when it was used as the anode material of a lithium ion battery. The electrochemical properties of the NiO/Co_3O_4 composite material were excellent. The material's discharge capacity during the first cycle was 2700 mAh·g^{-1} under a current of 100 mA·g^{-1}; a specific capacity of 400 mA h·g^{-1} was retained after 200 cycles; and the columbic efficiency could reach 99%.

Keywords: metal organic framework; lithium ion batteries; electrode material; NiO; Co₃O₄

1. INTRODUCTION

For energy, the world mainly relies on coal, oil, natural gas, and other nonrenewable energy sources, and all nonrenewable energy will eventually be exhausted. Therefore, how energy can be used and stored in a green and efficient manner is a crucial question. Lithium ion batteries (LIBs) are excellent energy storage devices because of their high theoretical capacity, long cycle life, rapid charging and discharging, no memory effect, small size, light weight, environmental friendliness, and nonpolluting. LIBs are widely used in electronics, electric vehicles, and large energy storage fields [1-4]. However, because of increasing demand, the energy density of LIBs must be further improved. One effective method is using metal organic frameworks (MOFs) as a new electrode material in LIBs [5]. An MOF combines metal and organic ligands through intermolecular hybridization and has the advantages of both metal and organic ligands; they can thus improve the capacity and cycle stability of LIBs [6]. Among the derivatives of MOFs, transition metal oxides (TMOs) are widely used in high-performance LIBs because of their high theoretical capacitance and good electrochemical stability [7-12]. Among the TMOs derived from MOFs, Co_3O_4 is considered to be an attractive electrode material for LIBs due to its theoretical capacitance of up to 980 mAh·g^{-1} [7]. MOFs have been prepared from Co_3O_4 with various morphologies—such as spherical dodecahedron nanostructures [13] and hollow dodecahedrons [14]—and then used as LIB electrode materials, exhibiting excellent electrochemical performance.

Compared with single-metal TMOs, those with multiple metal centers have higher metal proportion. The higher the metal content of TMOs, the more special properties they exhibit [15]. When two types of TMO are combined to form mixed TMOs, the storage capacity of lithium ions and conductivity can be significantly improved because two metal cations are present [16-20]. For example, $Co/CoFe_2O_4$ shell core structure was grown on carbon sheets in [20] for use in LIBs. A reversible capacity of 1127 mAh·g^{-1} was retained at after 50 cycles under a current of 100 mA·g^{-1}. Huang et al. reported a $Fe_2O_3@NiCo_2O_4$ nanocages delivered a capacity of 1079 mAh·g^{-1} at 100 mA·g^{-1} after 100 cycles [21]. Especially, some mixed TMO contained Co_3O_4 demonstrate evident enhanced lithium storage performance. A $Co_3O_4@TiO_2$ mixed TMO derived from ZIF-67 retained a reversible capacity of 642 mAh·g^{-1} after 200 cycles under a current of 500 mA·g^{-1} [22]. $Co_3O_4@$carbon composites, reported by Lin et al., can provide the specific capacity of 1050 mAh·g^{-1} after 50 cycles under specific current of 1C, which is higher than that of single Co_3O_4 particles [23]. A $Co_3O_4@$ carbon nanotube arrays, reported by Schth et al., can provide the specific capacity of 700 mAh·g^{-1} at 10 mA·g^{-1} after 100 cycles [24]

To obtain electrode materials with high energy density, NiO/Co_3O_4 composites were prepared using a hydrothermal method in which NiO nanosheets were combined with three-dimensional nano-Co_3O_4. This mixed transition metal oxide had large specific surface area due to its special flower-shape, therefore can provide more channels for Li ion transmission and more storage capacity of Li ion. The composite material has the advantages of both Ni and Co and has excellent electrochemical properties in that the Ni ions provided more electrochemical active sites.

2. EXPERIMENTAL

2.1 Materials

The materials used in this study included $Co(NO_3)_3 \cdot 6H_2O$, ethanol, $CO(NH_2)_2$, $Ni(NO_3)_2 \cdot 6H_2O$, deionized water, polyvinylidene difluoride (PVDF), acetylene black(ACET), and N-methyl-2-pyrrolidone (NMP).

The main instruments used were an electronic balance, centrifugal machine (TG16B), muffle furnace (GSL1500X), vacuum drying oven (DZF-6020), magnetic stirrer (DF-101S), X-ray diffraction (XRD) instrument (X'Pert PRO), scanning electron microscopy (SEM) instrument (Hitachis-SU8010), Land cell testing system (CT3001A), and electrochemical workstation (CHI660E).

2.2 Synthesis of NiO/Co_3O_4

First, 0.583 g of $Ni(NO_3)_2 \cdot 6H_2O$, 0.291 g of $Co(NO_3)_2 \cdot 6H_2O$ and 0.96 g of $CO(NH_2)_2$ were dissolved in 20 mL of deionized water, which was then magnetically stirred for 10 min. The fully dissolved solution was transferred to a Teflon-lined stainless steel autoclave. Subsequently, the autoclave was heated at 180°C for 8 h in an oven. The cooled solution was centrifuged four times to enable powder collection. The powders were dried at 60°C for 12 h in a vacuum and then calcined at 500°C for 3 h at a heating rate of $1°C \cdot min^{-1}$. After calcination, black NiO/Co_3O_4 composite powders were obtained. Fig. 1 shows the process of synthesizing the flower-like NiO/Co_3O_4 composite.
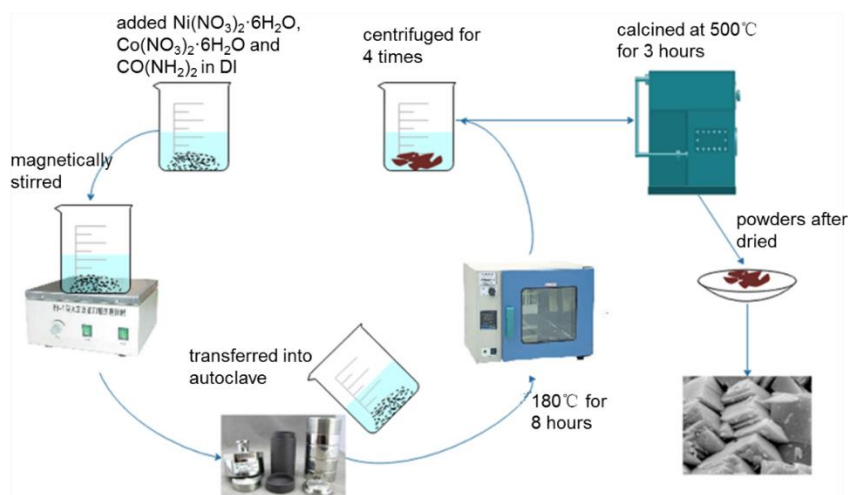

Figure 1. Synthesis of NiO/Co_3O_4.

3. RESULTS AND DISCUSSION

3.1 Morphology and phase analysis

The morphology of the prepared NiO/Co_3O_4 was determined using SEM (Fig. 2). The acceleration voltage was 30 kV, and the maximum magnification was 500 000× during scanning.

Crystallographic structure of the prepared NiO/Co_3O_4 was measured with Cu Kα radiation in a 2θ range from 30° to 70° by using XRD (Fig. 3).

Fig. 2(a) and 2(b) shows the morphology of NiO/Co_3O_4 before calcination and reveals that the NiO/Co_3O_4 compound was composed of flaky material with a flower-like shape. The compound's average radius was approximately 3 μm. The flower-like structure had not only regular morphology but also a large gap between flakes. However, because some suspicious residual conductive material was present on the surface, the material required calcination to remove impurities. Fig. 2(c) and 2(d) presents the morphology after calcination and shows a clearer flower morphology, which indicates that the impurities were removed as expected. The average radius of the complex remained approximately 3 μm, and the average thickness of each nanoscale flake was approximately 200 nm. This type of nanoscale flake with large gap can considerably improve the efficiency of lithium ion transmission during negative electrode reactions, improving the electrochemical properties of an LIB.
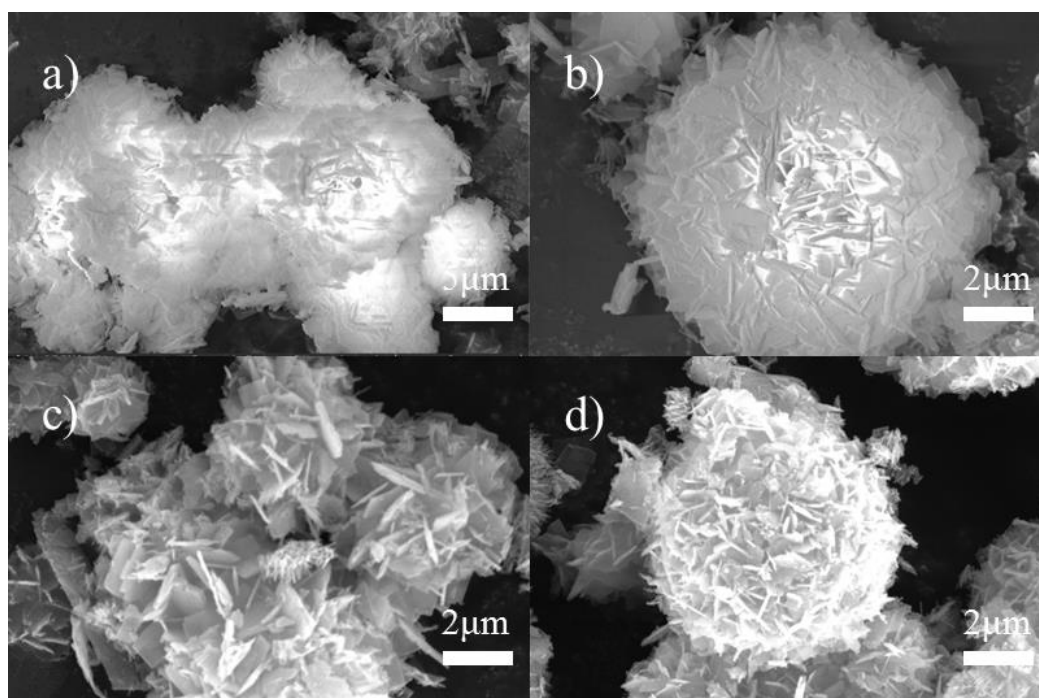

Figure 2. SEM images of NiO/Co_3O_4 before and after calcination.

The XRD pattern of NiO/Co_3O_4 is displayed in Fig. 3 (red line) and compared with the standard PDF card of Co_3O_4 and NiO. In the standard PDF card of Co_3O_4 (JCPDS: 42-1467), diffraction peaks occur at 31.5°, 37.0°, 37.9°, 56.0°, 58.9°, and 64.8°, corresponding to the (220), (311), (222), (422), (511), and (440) crystal planes, respectively. In the standard PDF card of NiO (JCPDS: 44-1159), the characteristic diffraction peaks are at 37.3°, 43.3°, and 62.8°, respectively corresponding to the (101), (012), and (110) crystal planes. The diffraction peaks in the NiO/Co_3O_4 spectrum perfectly match those of Co_3O_4 and NiO, indicating that Co_3O_4 and NiO retained their form in the NiO/Co_3O_4 composite, and no impurities were present. The Co_3O_4 lattice parameters a=b=c=8.062 Å are satisfied with standard XRD patterns of cubic Co_3O_4. The NiO lattice parameters a=b=2.905 Å, c=7.162 Å are greatly agreement with standard XRD patterns of rhombic NiO. It

indicated that the rhombic NiO is connected by the cubic Co_3O_4, and finally composed NiO/Co_3O_4 with a flower-like morphology.
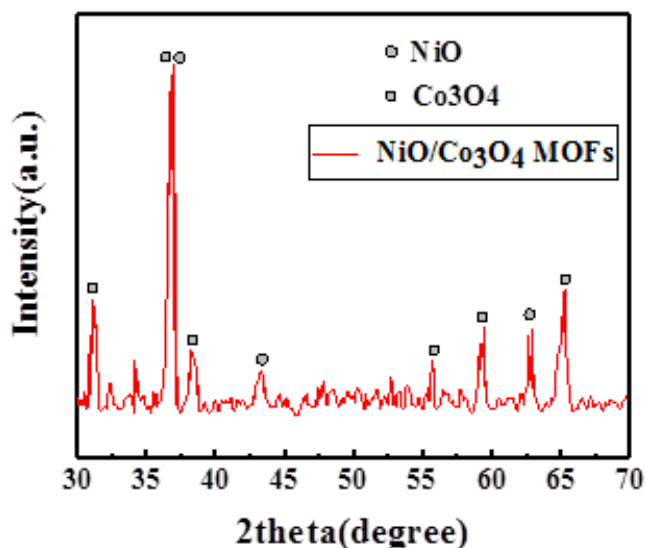

Figure 3. XRD pattern of NiO/Co_3O_4.

3.2 Electrochemical performance

In a weight ratio of 8:1:1, the NiO/Co_3O_4 composite, ACET, and PVDF were dissolved in NMP; the mixture was then magnetically stirred for 12 h. Subsequently, the stirred solution was evenly spread on a round copper sheet with a diameter of 15 mm, and the sheet was placed in a vacuum oven at 60℃ to dry. The dried copper sheet was used as the electrode in a half battery, which was assembled in an argon-filled glove box. The electrochemical performance of the half battery was analyzed through cyclic volt–ampere characteristic, specific capacity, coulombic efficiency, constant-current cyclic performance, rate capability, and impedance characteristic testing on the Land cell testing system and an electrochemical station.

The electrochemical reactions of NiO and Co_3O_4 with Li are stated as below [22, 25]:

$$Co_3O_4 + 8Li^+ + 8e^- = 4Li_2O + 3Co \tag{1}$$

$$NiO + 2Li^+ + 2e^- = Li_2O + Ni \tag{2}$$

The cyclic voltammetry (CV) curves of the first four cycles are displayed in Fig. 4(a). The test voltage range was 0.1–3.00 V, and the scanning speed was 0.0001 $mV·s^{-1}$. For the first cycle of the discharge period, two clear reduction peaks were present at 0.49 and 0.8 V; the 0.49 V peak is slightly larger than that at 0.8 V and corresponds to the reduction of Ni^{2+} to Ni during the discharge process [25], whereas the smaller reduction peak at 0.8 V corresponds to the reduction of cobalt ions to Co during the discharge period [22]. When Ni^{2+} was reduced to Ni, a solid electrolyte interface (SEI) membrane was formed. During the first charging cycle, a relatively clear oxidation peak at 2.25 V and small oxidation peak at 1.55 V were obtained. The oxidation peak at 2.25 V corresponded to Ni oxidation to Ni^{2+} [25], whereas that at 1.55 V corresponded to the formation of cobalt ions [22].

Because an SEI membrane formed, the battery capacity declined irreversibly. Compared with the first cycle, the height of the oxidation and reduction peaks in the second cycle was significantly shorter, and the reduction peak was slightly shifted to the right which exhibiting a small polarization [25]. The integral area was also considerably smaller than that in the first cycle, which indicated that the specific capacity is decreased. In the second cycle of discharge, a reduction peak was discovered at 0.9 V, which corresponded to Co^{2+} turning into Co; the reduction peak of other valence cobalt ions reducing to cobalt was negligible. The reduction peak at 0.49 V decreased significantly in the second cycle, which is due to the poor conductivity of NiO and the pulverization of NiO particles [25]. Additionally, fewer oxidation and reduction peaks occurred. The main reason was that when Co was changed to Co ions during sintering, various valence states of cobalt were formed, but in the charging period of the first cycle, Co mostly turned into Co^{2+}, resulting in the barely noticeable reduction and oxidation peaks of other Co ions during the first two cycles. In the third and fourth circles, the height of the oxidation and reduction peak is still decreasing, but the variation is tended to be stable. The integral area showed same change tendency. These CV results are good consistent with the specific capacity curves.

To test the specific capacity and coulomb efficiency of a NiO/Co_3O_4 LIB after multiple cycles, the NiO/Co_3O_4 LIB was charged and discharged under a current density of 200 $mAh·g^{-1}$ from 0.01 to 3.00 V for 100 cycles. The test results are presented in Fig. 4(b). The battery's specific capacity in the first cycle was 2700 $mAh·g^{-1}$, but it decreased rapidly during the first 15 laps. After the 15th cycle, it decreased slowly and almost stabilized. The lowest specific capacity was 190 $mAh·g^{-1}$, which was reached after 80 cycles.

In the first lap, the structure of NiO/Co_3O_4 is intact and there is no SEI membrane to hinder the lithium ion transmission, so the specific capacity is the highest. The sharp decrease in the discharge specific capacity during the first 15 cycles was because of the SEI membrane and the greatly volume change of NiO/Co_3O_4 during the cycles, which caused severe particle condensation and low intrinsic conductivity [26]. The slow decrease in capacity during cycles 15 to 100 indicated that lithium ions failed to emerge after embedding due to the electrode's structure and limited contact area of the electrode material with the electrolyte. However, after cycle 100, the discharge specific capacity slowly rebounded because the structure of the Li_2O embedded electrode material stabilized and the number of lithium ions that could be transmitted in the electrolyte increased slightly.

Fig. 4(c) shows the charging and discharging test results for the 1st, 5th, 15th, and 20th charge–discharge cycles under a current of 200 $mA·g^{-1}$. Initially, the discharge capacity was 2700 $mAh·g^{-1}$, charging specific capacity was 800 $mAh·g^{-1}$, and corresponding coulomb efficiency was 28.5%. During the first discharge period, the voltage decreased rapidly to a voltage platform of approximately 500 mV and then slowly to a cutoff voltage of 190 mV. The curve was reasonably consistent with the CV results. In the subsequent charge–discharge cycles, the specific capacity decayed rapidly due to the formation of an SEI membrane and the aforementioned dramatic volume change of NiO [27]. In the fifth cycle, the discharge capacity was approximately 800 $mAh·g^{-1}$, and the charging capacity was approximately 600 $mAh·g^{-1}$, but the coulomb efficiency rapidly increased to 75%. After the 15th cycle, the charge and discharge capacity decreased more slowly than previously.

Fig. 4(d) shows the capacity under a current density of 200, 400, 800, 1200, 1600, and 2000

mA·g^{-1}. As the current density was increased, the capacity was decreases. Under the current density of 1200 mA·g^{-1}, discharge specific capacity is only 150 mAh·g^{-1}. Therefore, the NiO/Co$_3$O$_4$ LIB is not recommended for use under a high current density. But the capacity was approximately 400 mAh·g^{-1} when the current density was set back to 200 mA·g^{-1}, which was not only a restoration to the original specific capacity but to a slightly higher capacity. It indicated that NiO/Co$_3$O$_4$ has excellent reversible property.

In electrochemical impedance spectroscopy measurements, the initial voltage was 2.8 V. The test results, shown in Fig. 4(e), show a line composed of two parts: a high-frequency area on the left and low-frequency area on the right. The high-frequency area is related to the charge transfer process, whereas the low-frequency region is related to the LIB conduction process [22]. From the test results, the charge transfer resistance can be clearly observed to be approximately 70 Ω, which is smaller than pure Co$_3$O$_4$. Thus, the NiO/Co$_3$O$_4$ material had low impedance and high charge transmission efficiency, indicating that the lithium ions can easily embed and disengaged from NiO/Co$_3$O$_4$.
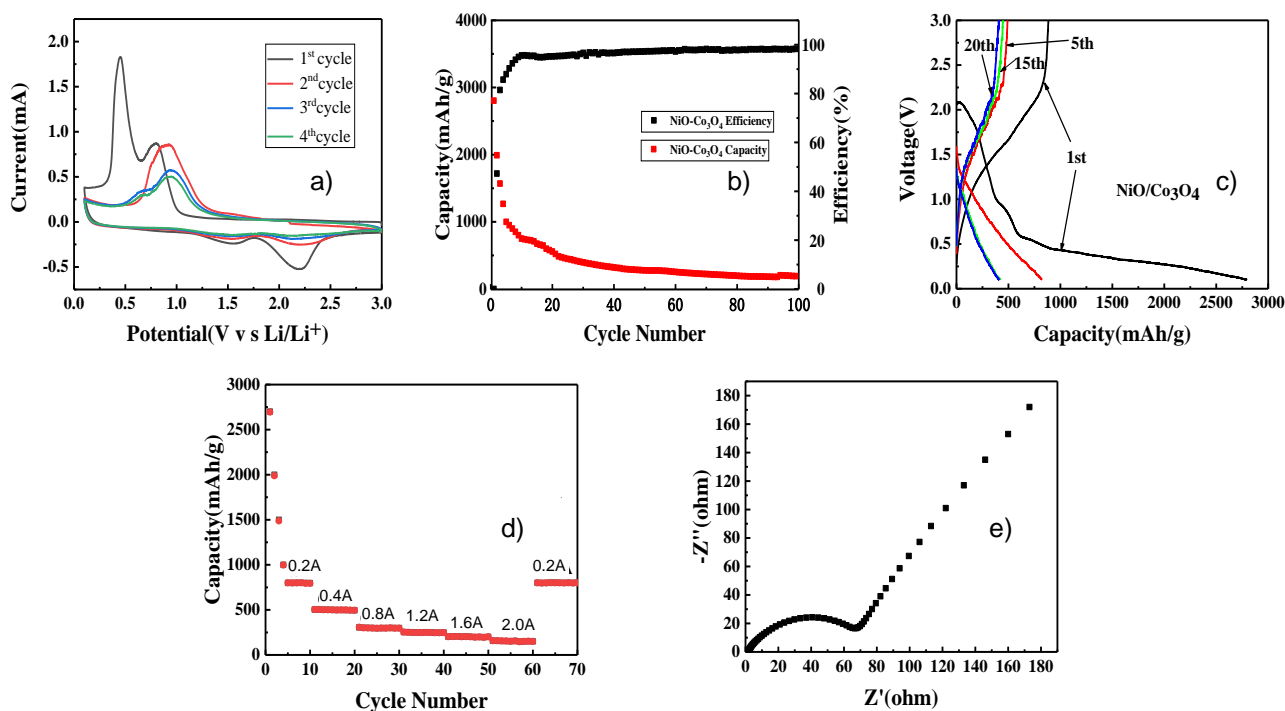

Figure 4. Electrochemical performance of NiO/Co$_3$O$_4$: (a) CV curves. (b) Cycling performance and coulombic efficiency. (c) Constant-current charge–discharge curves. (d) Rate capability at various current densities. (e) Impedance curves.

Table 1 compares some electrochemical parameters of Co$_3$O$_4$@TiO$_2$ described in [22], Co/CoFe$_2$O$_4$ in [20], and NiO/Co$_3$O$_4$ in this paper. The NiO/Co$_3$O$_4$ had the highest initial specific capacity and average capacity under a current density of 200 mA·g^{-1} along with the lowest charge transfer resistance. However, its specific capacity was lower than that of the other two materials. The data in Table 1 indicate that NiO/Co$_3$O$_4$ provides an extremely high initial specific capacity, coulomb efficiency, and average capacity under a low current.

Table 1. Electrochemical parameter comparison.

Materials	Initial specific capacity (mAh·g^{-1})	Specific capacity after 50 cycles (mAh·g^{-1})	Average capacity under 0.2A·g^{-1} (mAh·g^{-1})	Charge transfer resistance (ohm)
Co/CoFe$_2$O$_4$@C[20]	1677	1150	780	80
Co$_3$O$_4$@ TiO$_2$[22]	662	580	620	80
NiO/Co$_3$O$_4$	2700	400	800	70

4. CONCLUSION

In this paper, a flower-like NiO/Co$_3$O$_4$ composite was prepared using a hydrothermal method. The regular flower shape and large gap were clearly observed in SEM images. The composite's special morphology resulted in high-efficiency lithium ion transmission in the negative electrode reaction. NiO and Co$_3$O$_4$ structures in the composites were identified using XRD analysis, indicating that the experiment performed in this study was reasonable. The SEM result indicated that the crystal shape was not changed by calcination. The flower-like NiO/Co$_3$O$_4$ material was used as an electrode in an LIB, and various electrochemical performance tests were performed. The results revealed that the initial specific capacity was 2700 mAh·g^{-1}, the specific capacity was stable at 400 mAh·g^{-1} after 200 cycles, and the coulomb efficiency could reach 99%.

References

1. M. Armand and J. M. Tarascon, *Nature,* 451(2008) 652.
2. J. W. Choi and D. Aurbach, *Nat. Rev. Mater.*, 1(2016)16013.
3. R. F. Service, *Science*, 344(2014),352.
4. J. M. Tarascon and M. Armand, *Nature*, 414(2001)359.
5. G. X. Zheng, M. H. Chen, J. H. Yin, H. R. Zhang, X. Q. Liang and J. W. Zhang, *Int. J. Electrochem. Sci.,* 14(2019) 2345.
6. Z. Q. Xie, W. W. Xu, X. D. Cui and Y. Wang, *Chem. Sus. Chem.*, (2017)1645.
7. C. S. Yan, G. Chen, X. Zhou, J. X. Sun and C. Lv, *Adv. Funct. Mater.*,26(2016) 1428.
8. Y. Ren, Z. Liu, F. Pourpoint, A. R. Armstrong, C. P. Grey and P. G. Bruce, *Angew. Chem. Int. Ed.*, 51(2012)2164.
9. X. W. Lou, Y. Wang, C. Yuan, J. Y. Lee and L. A. Archer, *Adv. Mater.*,18(2006)2325.
10. X. J. Zhu, Y. W. Zhu, S. Murali, M. D. Stoller and R. S. Ruoff, *ACS Nano*,5(2011)3333.
11. M. Ahmad, S. Yingying, A. Nisar, H. Y. Sun, W. C. Shen, M. Wei and J. Zhu, *J. Mater. Chem.*, 21(2011)7723.
12. S. Ko, J. I. Lee, H. S. Yang, S. Park and U. Jeong, *Adv. Mater.*, 24(2012)4451.
13. J. Shao, Z. M. Wan, H. M. Liu, H. Y. Zheng, T. Gao, M. Shen, Q. T. Qu and H. H. Zheng, *J. Mater. Chem.* A, 2(2014)12194.
14. R. B. Wu, X. K. Qian, X. H. Rui, H. Liu, B. L. Yadian, K. Zhou, J. Wei, Q. Y. Yan, X. Q. Feng, Y. Long, L. Y. Wang and Y. Z. Huang, *Small*, 10(2014)1932.
15. Q. Song and Z. J. Zhang, *J. Am. Chem. Soc.*, 134(2012)10182.
16. G. Huang, L. L. Zhang, F. F. Zhang and L. M. Wang, *Nanoscale*, 6(2014)5509.
17. G. Huang, F. F. Zhang, L. L. Zhang, X. C. Du, J. W. Wang and L. M. Wang, *J. Mater. Chem.* A, 2(2014)8048.
18. H. Guo, T. T. Li, W. W. Chen, L. X. Liu, X. J. Yang, Y. P. Wang and Y. C. Guo, *Nanoscale*,

    6(2014)15168.
19. F. C, Zheng, D. Q. Zhu, X. H. Shi and Q. W. Chen, *J. Mater. Chem*. A, 3(2015)2815.
20. Q. Q. Dou, Y. Li and K. Ming, *J. Alloys Compd.*, 808 (2019)151691.
21. G. Huang, L. L. Zhang, F. F. Zhang and L. W. Wang, *Nanoscale*, 6(2014)5509.
22. W. W. Xu, X. D. Cui, Z. Q. Xie, G. Dietrich and Y. Wang, *Electrochim. Acta*, 222 (2016)1021.
23. Y. Wang, H. J. Zhang, L. Lu, L. P. Stubbs, C. C. Wong and J. Y. Lin, *ACS Nano,* 4(2010)4753.
24. D. Gu, W. Li, F. Wang, H. Bongard, B. Spliethoff, W. Schmidt, C. Weidenthaler, Y. Y. Xia, D.Y. Zhao and F. Schüth, *Angew. Chem. Int. Ed.,* 54(2015)7060.
25. X. H. Huang, J. P. Tu, C. Q. Zhang and F. Zhou, *Electrochim Acta*, 55(2010)8981.
26. P. Poizot, S. Laruelle, S. Grugeon, L. Dupont and J. Tarascon, *Nature,* 407(2000)496.
27. M. A. Rahman and C. Wen, *Ionics,* 21(2015)2709.